Behavioral/Systems/Cognitive

Power Fluctuations in Beta and Gamma Frequencies in Rat Globus Pallidus: Association with Specific Phases of Slow Oscillations and Differential Modulation by Dopamine D_1 and D_2 Receptors

Cyril Dejean,[1,2,4] Gordon Arbuthnott,[1,3] Jeffery R. Wickens,[1,3] Catherine Le Moine,[4] Thomas Boraud,[5,6] and Brian I. Hyland[2]

Departments of [1]Anatomy and Structural Biology and [2]Physiology, School of Medical Sciences, University of Otago, Dunedin 9054, New Zealand, [3]Okinawa Institute for Science and Technology, Okinawa, Japan 904-0412, [4]Université de Bordeaux 1, Institut des Neurosciences Cognitives et Intégratives d'Aquitaine, Centre National de la Recherche Scientifique, (CNRS) Unité Mixte de Recherche (UMR) 5287, F-33000 Bordeaux, France, [5]Université de Bordeaux, Institut des Maladies Neurodégénératives, UMR 5293, F-33000 Bordeaux, France, and [6]CNRS, Institut des Maladies Neurodégénératives, UMR 5293, F-33000 Bordeaux, France

Modulation of oscillatory activity through basal ganglia–cortical loops in specific frequency bands is thought to reflect specific functional states of neural networks. A specific negative correlation between beta and gamma sub-bands has been demonstrated in human basal ganglia and may be key for normal basal ganglia function. However, these studies were limited to Parkinson's disease patients. To confirm that this interaction is a feature of normal basal ganglia, we recorded local field potential (LFP) from electrodes in globus pallidus (GP) of intact rats. We found significant negative correlation between specific frequencies within gamma (≈60 Hz) and beta (≈14 Hz) bands. Furthermore, we show that fluctuations in power at these frequencies are differentially nested within slow (≈3 Hz) oscillations in the delta band, showing maximum power at distinct and different phases of delta. These results suggest a hierarchical organization of LFP frequencies in the rat GP, in which a low-frequency signal in the basal ganglia can predict the timing and interaction of power fluctuations across higher frequencies. Finally, we found that dopamine D_1 and D_2 receptor antagonists differentially affected power in gamma and beta bands and also had different effects on correlation between them and the nesting within delta, indicating an important role for endogenous dopamine acting on direct and indirect pathway neurons in the maintenance of the hierarchical organization of frequency bands. Disruption of this hierarchical organization and subsequent disordered beta–gamma balance in basal ganglia disorders such as Parkinson's disease may be important in the pathogenesis of their symptoms.

Introduction

Oscillatory synchronization of neuronal assemblies is thought to enable periodic functional linkages between brain areas for specific information processing (Buzsáki et al., 1994; Singer, 2001; Fries et al., 2002, 2007). In neural circuits of the basal ganglia, modulation of oscillatory activity at different frequencies is particularly important for normal processing (Brown et al., 2002; Courtemanche et al., 2003; Berke et al., 2004).

Data from recordings in human subthalamic nucleus (STN) have shown that the power in gamma and beta sub-bands is negatively correlated, in the absence of movement (Fogelson et al., 2005). This suggests the possibility that a regulatory mechanism controls the power relationship between these bands within a single behavioral state, over and above any alternation in power that may occur across different movement states. Furthermore, in other brain regions not directly within the basal ganglia, evidence is accumulating for phase–amplitude coupling between low- and high-frequency oscillations. This has been interpreted as reflecting a fundamentally hierarchical organization of oscillatory frequencies (Bragin et al., 1995; Lakatos et al., 2005; Sirota and Buzsáki, 2005; Canolty et al., 2006; Isomura et al., 2006; Mena-Segovia et al., 2008; Sirota et al., 2008). However, the human STN data were obtained from patients with Parkinson's disease, leaving the possibility that the results reflected this pathology. The first aim of the present study was therefore to determine whether such hierarchical organization of frequencies occurs in the normal basal ganglia.

If such a hierarchical organization exists, an additional question of interest is the role of dopamine D_1 and D_2 receptors in regulating it. The striatum, STN, and the globus pallidus (GP) all

Received May 28, 2009; revised Feb. 21, 2011; accepted Feb. 24, 2011.

Author contributions: C.D., G.A., J.R.W., and B.I.H. designed research; C.D. performed research; C.L.M. and T.B. contributed unpublished reagents/analytic tools; C.D., C.L.M., T.B., and B.I.H. analyzed data; C.D., G.A., J.R.W., and B.I.H. wrote the paper.

This work was supported by the New Zealand Neurological Foundation and Health Research Council. We thank Aaron Sheerin and Roseanna Smither for technical assistance.

Correspondence should be addressed to Assoc. Prof. Brian Hyland, Department of Physiology, School of Medical Sciences, University of Otago, P.O. Box 913, Dunedin 9054, New Zealand. E-mail: brian.hyland@otago.ac.nz.

DOI:10.1523/JNEUROSCI.3311-09.2011

 0270-6474/11/316098-10$15.00/0

receive dopaminergic input (Smith et al., 1998; Gauthier et al., 1999). Dopamine D_1 and D_2 receptors are very highly expressed in the basal ganglia but differentially in the direct and indirect pathways (Surmeier et al., 2007). The D_1 receptor is found on "direct" pathway striatal neurons that project to the internal globus pallidus. In contrast, the D_2 receptor dominates in the "indirect" pathway, which passes through the external GP and STN (Smith et al., 1998). Interaction between the tightly interconnected GP and STN (Bevan et al., 2002) has been proposed as an engine for basal ganglia oscillations (Plenz and Kital, 1999; Humphries et al., 2006), raising the possibility of a special role for D_2 receptor in the regulation of basal ganglia rhythmic activity by dopamine. We therefore further investigated whether D_1 and D_2 receptors have differential roles in modulating basal ganglia oscillatory activity, using selective receptor antagonists.

Materials and Methods

All procedures were approved by the Animal Ethics Committee at the University of Otago (approval 59/04) and conducted in accordance with the New Zealand Animal Welfare Act. Eleven male Wistar rats weighing 250–400 g at the time of surgery were used for the main study. Food and water were available *ad libitum* in the home cage, and experiments were performed during the dark portion of a reversed 12 h light/dark cycle.

Recording electrodes were implanted after at least 7 d of daily handling habituation, under full general anesthesia [70 mg/kg ketamine and 0.5 mg/kg Domitor (medetomidine HCl), s.c.] with local anesthetic (0.5% Marcaine) at the incision site and under prophylactic antibiotic [Procaine Penicillin G and dihydrostreptomycin sulfate (Strepcin), 1 ml/kg, s.c.]. The recording electrodes [eight 0.001-inch coated diameter Formvar-insulated nichrome microwires (A-M Systems), fixed in a 30-gauge stainless-steel cannula] were lowered to position through a small craniotomy. The electrode tips were targeted to the dorsal margin of the left GP (1.1 mm posterior to bregma, 3.1 mm lateral to midline, and 5.0 mm below the dura surface) and advanced by small steps ($\approx$50 μm) each day using an on-head microdrive. Seven stainless-steel skull screws were inserted, and the implant was affixed to the skull with dental acrylic. A contralateral skull screw positioned over the cerebellum ~14 mm caudal of bregma was used for animal ground connection. Animals were injected with the sedation-reversal agent Antisedan (atipamezole HCl, 1.25 mg/kg, s.c.) and allowed to recover before being returned to the animal housing facilities.

Beginning 5 d after surgery, the electrodes were advanced daily in small increments for 2–3 weeks, until the tips reached the depth coordinate for the center of the GP. Electrode positions were marked at the end of the experiments by electrolytic lesions (10–50 mA direct current for 20–30 s), and only those animals with tips confirmed within the GP were included in analysis.

Recordings were made within a clear acrylic box in a dimly lit room. After connection of the recording cable (incorporating impedance-matching unity-gain amplifiers), animals were allowed to settle for 15–20 min. Recordings of local field potentials (LFPs) were then made for 10 min before (predrug) systemic injection of raclopride, SCH23390 [*R*(+)-7-chloro-8-hydroxy-3-methyl-1-phenyl-2,3,4,5-tetrahydro-1*H*-3-benzazepine hydrochloride], or vehicle and again for 10 min, beginning 5 min after the injection (postdrug). LFP recordings were made from the single electrode with the best signal-to-noise ratio in single-ended mode (referenced to amplifier signal ground), bandpass filtered (0.1–400 Hz; Axon CyberAmp 380 signal conditioner; Molecular Devices), digitized at 1 kHz (Power1401 data-acquisition system; Cambridge Electronic Design), and recorded using Spike2 software (Cambridge Electronic Design). The bandpass filters for other wires in the bundle were set at 0.5–10 kHz, in case single neurons were present.

In a separate group of three animals, 0.001-foot nichrome wire tetrodes were used instead of bundled single wires to improve yield of single unit spikes. Raw data were initially recorded as wide band (0.1 Hz to 20 kHz) signals and split into two copies; one was downsampled to 1 kHz for LFP analysis and the other bandpass filtered (100 Hz to 20 kHz) for spike waveform detection (supplemental data, available at www.jneurosci.org as supplemental material). This allowed spiking and LFP to be analyzed from the same electrodes. Data from this group were used to check for phase relationship of cell spiking activity with locally recorded LFP.

Drugs were dissolved in 0.9% saline and administered intraperitoneally. Raclopride (Sigma-Aldrich), a selective dopamine D_2 antagonist, was dissolved at 1.0 mg/ml and the selective D_1 antagonist SCH23390 (Sigma-Aldrich) at 0.5 mg/ml with both drugs administered in a volume of 1.0 ml/kg for final doses of 1.0 and 0.5 mg/kg, respectively. It was important for the present study that the behavioral effect of the two drugs was matched to allow comparisons and that the behavioral state was stable for the period of the recordings. Doses of the two drugs were chosen on the basis of preliminary experiments as sufficient to produce a comparable cataleptic response [similar levels of akinesia measured by the bar test (Marin et al., 1993)] and are higher than required to affect operant behavior. At this dose, SCH23390 remains selective for D_1 over D_2 receptors (Bischoff et al., 1986). Saline injected at 1.0 ml/kg served as a negative control. Drug tests were made at least 2 weeks apart.

The animals were continuously monitored during data acquisition, and activity periods were marked on an event channel of the recorded data file using keystroke input. Example traces are shown in supplemental Figure S1 (available at www.jneurosci.org as supplemental material). During postdrug catalepsy, animals were primarily akinetic. Movement can be a powerful modulator of power in gamma and beta bands, as is illustrated in supplemental Figure S2 (available at www.jneurosci.org as supplemental material). Therefore, to ensure that predrug–postdrug comparisons were not confounded by changes in the level of movement, analysis was limited to periods of immobility (no locomotion, rearing, or grooming) of at least 3 min duration, from within the 10 min predrug and postdrug recording periods. Thus, all postdrug data were obtained from within a time window extending from 5 to 15 min after injection. Periods with high voltage spindles were excluded in the recordings. Animals remained upright, and, although rapid eye movement sleep episodes cannot be ruled out, large-amplitude slow waves typical of slow-wave sleep were not observed. For each animal, the selected predrug and postdrug periods were of equal lengths.

The level of akinesia achieved by drug administration was quantified at the end of the postdrug recording period (i.e., 15 min after injection) using the bar test (Marin et al., 1993). For this, the animal's front paws were placed on a horizontal bar 10 cm above the bench, and the time until a single paw moved from the bar was recorded, to a maximum of 120 s.

Frequency spectrum analysis. A second-order Butterworth band-stop filter with settings 49 and 51 Hz (Matlab; MathWorks) was used to remove 50 Hz mains interference. The power spectral density (PSD) of the LFP was then computed using fast Fourier transform (FFT), with the Welch spectral estimator and a Hamming window of 2048 points (2 s) with 50% overlap and 1 Hz resolution. A significant peak in the power spectrum was defined as four consecutive increasing power values.

Power correlation analysis. We analyzed the temporal correlation between spectral power at different frequencies f as described previously (Masimore et al., 2004), by computing the time-resolved PSD of the LFP. The appropriate time resolution for evolving PSD to capture power fluctuations of beta and gamma was determined from inspection of the raw signal, and was set at 50 ms. We used FFT with a 75% overlapping Hamming window of 200 points (0.2 s) in the 0.1–1000 Hz range with 1 Hz resolution, with each window representing a single time point in the time-resolved PSD. This window size does not allow analysis of oscillations with period <200 ms, so the present analysis was limited to frequencies between 5 and 100 Hz. This generated time series of power values [$P_{f1,I}$, $P_{f1,i+1}$, $P_{f1,i+n}$…; $P_{f2,I}$, $P_{f2,i+n}$; etc.] corresponding to each 50 ms epoch I, for each frequency f. Because power values are not Gaussian, we calculated the nonparametric Spearman's rank correlation ($\rho_{(f1,f2)}$) for all possible pairs of power time series, generating two-dimensional matrices of negative and positive spectral correlations for each animal. The significance of the negative and positive correlation values were calculated using the nonparametric Fisher's test.

Gabor analysis. We used Gabor functions to further investigate temporal fluctuations in power in LFP bands. Gabor functions are commonly used to fit autocorrelation (AC) and cross-correlation histograms of nonstationary rhythmic biological time series such as neuronal spiking activity (Gray et al., 1989; Engel et al., 1990; Young et al., 1992). For our LFP

analysis, they are damped sine waves, with two terms, first the sine wave frequency (f_o), the amplitude of which is modulated by the second term, here the damping frequency (f_d). The Gabor functions served as predicted AC (pAC), used to fit the actual AC of the LFP frequencies of interest.

We constructed a set of Gabor functions as follows (Young et al., 1992; Nargeot et al., 2007):

$$\mathrm{pAC}_{f_o f_d}(x) = \cos(2\pi \times x \times f_o) \times \exp(C \times x^2 \times f_d), \quad (1)$$

with f_o and f_d both ranging from 1 to 100 Hz, hence creating 100 × 100 predicted AC. The quality of the fit of each predicted AC was then assessed by its correlation (Spearman's ρ) with the actual AC of specific LFP bands (calculated for lags t of 0–500 ms), and this correlation score was plotted for each f_o,f_d pair. Points showing the highest correlation thus represent candidate f_o,f_d pairs capable of predicting fluctuations in LFP power.

Perievent time power spectral analysis. To determine whether fluctuations in LFP power were linked to a specific phase of candidate f_d frequencies revealed by the Gabor analysis, we generated averaged perievent time power spectra (PETPS). In these PETPS, the power of each frequency was calculated over lags of ±0.5 s with respect to the troughs in the candidate f_d from 100 s of data for each animal. First, PSD (1 Hz resolution) were computed for 75% overlapping Hamming windows of 200 points (0.2 s), for 1 s periods centered on each trough. These individual PSD were then averaged to generate the PETPS for each animal. Finally, to compute unbiased group average data, the power values for each animal were normalized by converting to z-scores ($z\mathrm{PETPS}_f$), as follows:

$$z\mathrm{PETPS}_f(t) = \frac{\mathrm{PETPS}_f(t) - \overline{\mathrm{PETPS}_f}}{\sigma_{\mathrm{PETS}_f}}, \quad (2)$$

where f denotes the frequency component being analyzed, and t is time relative to the trigger. These zPETPS values were then averaged across animals.

To quantify the relationships suggested by the PETPS analysis, we computed the phase of maximum power with respect to the candidate f_d using the Hilbert transform in Matlab, with LFP troughs set to 0° phase. We then determined the local power maxima within 0° and 360° of the trough. The mean phase value for the maximum was calculated for each rat, and the distribution across all rats was analyzed. The presence of a significant preferred phase was tested using the Rayleigh's test for directional data (Fisher, 1993). For this, the 0–360° circular space was divided into 12 bins of equal size, giving an angular resolution of 30°. The Rayleigh's test is based on the hypothesis that phases of power maxima are uniformly distributed along the circular space. The presence of a significant preferred phase of a given frequency was calculated for data before injection of saline (control) and after saline, SCH23390, and raclopride injections. We assessed the effect of each drug on the preferred phase using the Watson's U^2 test (Fisher, 1993).

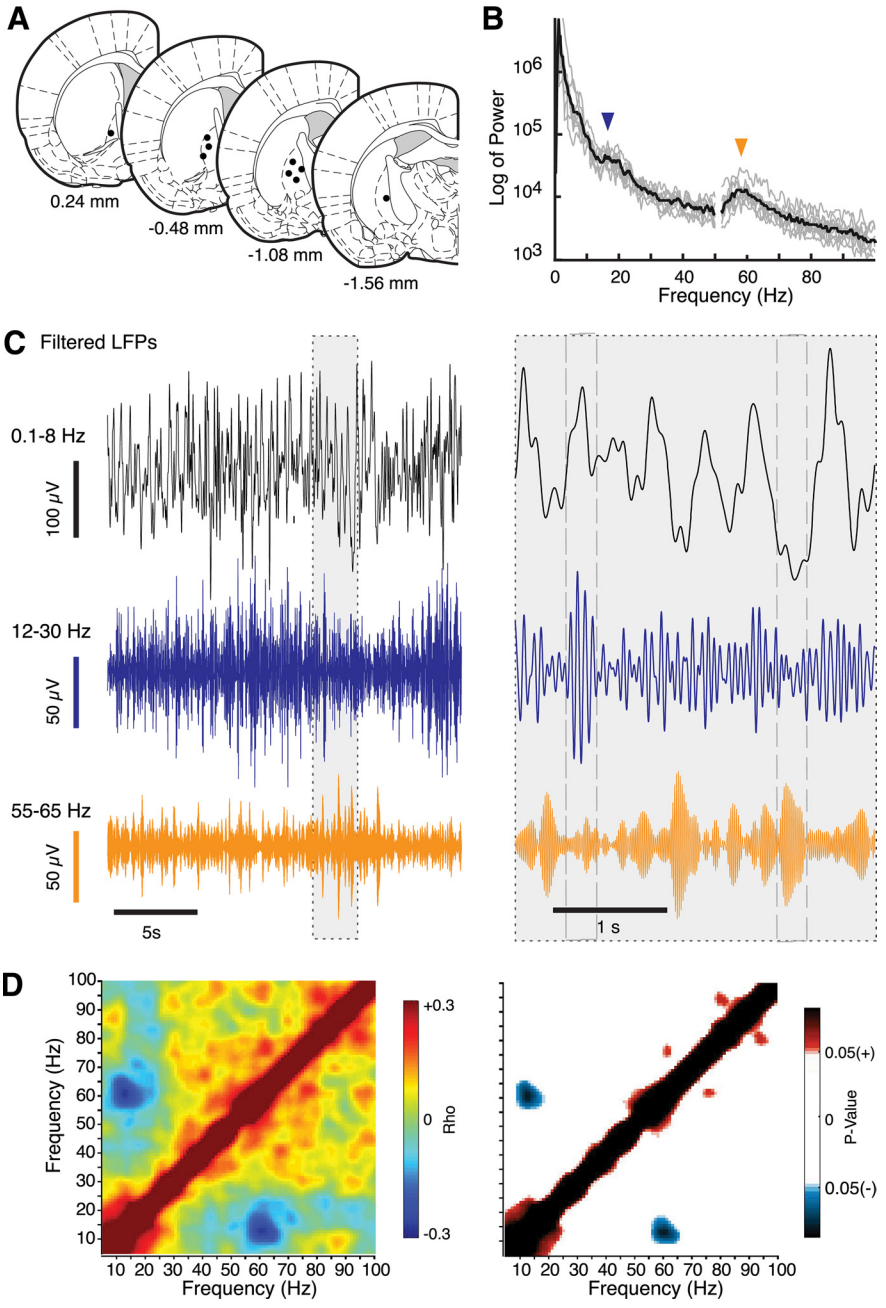

Figure 1. Globus pallidus local field potentials. ***A***, Diagrams of brain sections (adapted from Paxinos and Watson, 1997) show positions of recording electrode tips. ***B***, Black line shows population average ($n = 9$ animals) and gray lines individual animal power spectral density of LFP recorded during quiet rest. Arrowheads indicate peaks at ≈14 and ≈60 Hz. ***C***, Example filtered LFP showing activity in 0.1–8, 12–30, and 55–65 Hz bands. Right shows expanded view of the gray section from left. Dashed lines highlight periods of reciprocal variation in amplitude of oscillations at 12–30 and 55–65 Hz bands, associated with particular phases of the 0.1–8 Hz band. ***D***, Power correlation matrix for one animal calculated across the entire record, confirming significant negative interaction of power of oscillations. Left matrix color scale shows Spearman's coefficient of correlation (ρ), for all possible frequency pairs. Right matrix shows frequency pairs from ***A*** that had significant ($p < 0.05$) negative (blue) or positive interactions (red).

Results

We recorded LFP in the GP of nine Wistar rats with confirmed electrode positions (Fig. 1*A*). Spectral analysis of LFP revealed two distinct peaks (Fig. 1*B*). One was located between 13 and 17 Hz across animals, with a mean ± SD of 14.8 ± 1.3 (low beta). We refer to this frequency component as β_{14}. The second peak was found within the gamma band at 54–61 Hz across animals, with a mean of 59.3 ± 2.4 Hz, and is referred to here as γ_{60}. The frequency spectrum was also characterized by the presence of considerable power density

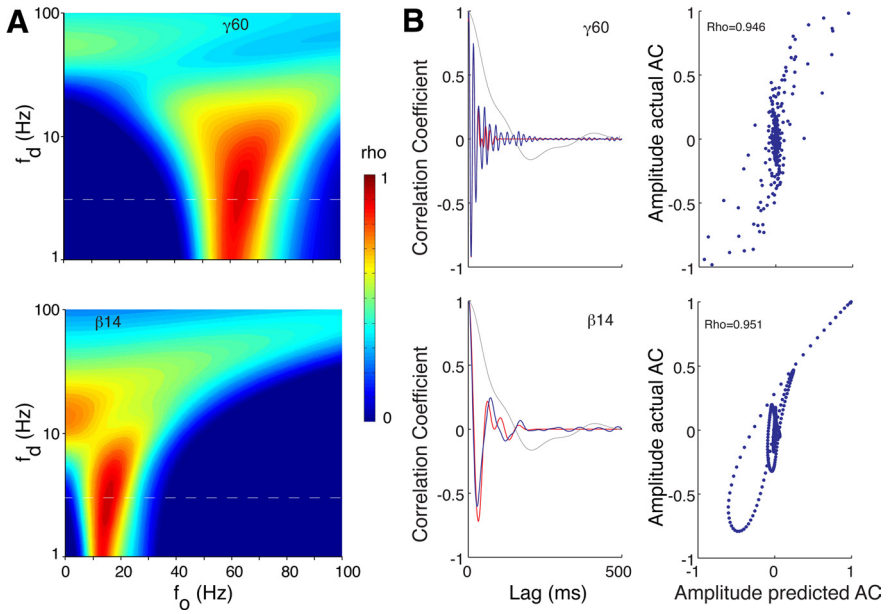

Figure 2. Slow LFP oscillations predict amplitude fluctuations in higher-frequency bands. ***A***, Matrices show mean ($n = 9$ animals) Spearman's ρ values (color scale) for the correlations between the actual AC for γ_{60} (top) and β_{14} (bottom) and predicted AC generated by Gabor functions from different combinations of f_o (pure sine wave, *x*-axis linear scale) and f_d (damping frequency, *y*-axis log scale) terms. White dashed line indicates $f_d = 3$ Hz. ***B***, Left show predicted AC (red lines) with $f_d = 3$ Hz for $f_o = 60$ Hz (top) and 14 Hz (bottom), overlaid on the actual AC (blue lines) for γ_{60} and β_{14} LFP recorded from one rat. Gray line shows the autocorrelation for the delta (0.1–3 Hz) band. Right scatter plots show the actual and predicted AC amplitudes, at all lags, for the data in the left, and the respective correlation coefficient (Spearman's ρ).

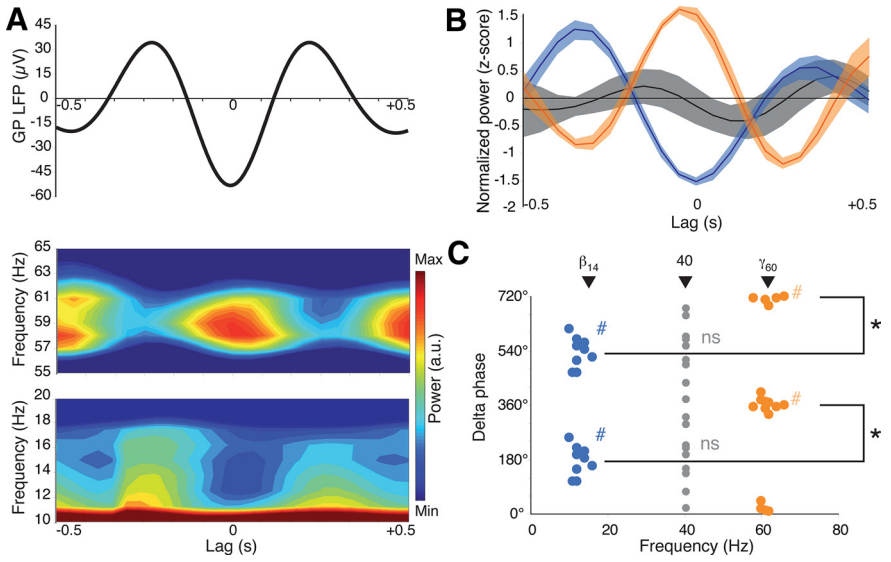

Figure 3. Fluctuations in power of specific frequencies nest within slow oscillations. ***A***, Waveform shows average delta (0.1–3 Hz) bandwidth filtered LFP, triggered on trough, for one rat. Color PETPS plots show examples of fluctuations in power in higher-frequency bands (top, 55–65 Hz; bottom, 10–20 Hz), around the delta trough. Power shown by color scale in arbitrary units (a.u.). ***B***, Group data. Color bands show the average ± SEM normalized (*z*-score, $n = 9$ rats) trough-triggered perievent-time power at β_{14} (blue), γ_{60} (orange), and 40 Hz (gray). ***C***, Points show the delta phase (0 = trough) at which maximum power occurs for β_{14}, γ_{60}, and 40 Hz, for each animal. $^{\#}p < 0.05$ compared with random distribution (Rayleigh's test); $^{*}p < 0.05$ comparing delta phase distributions of different frequencies (Watson's U^2 test).

at slower oscillatory frequencies, peaking in different animals at frequencies between 0.1 and 10 Hz but with no particular preferred frequency in this range.

These recordings were made with fixed bandpass optimized for LFP, so it was not possible to record action potential spikes on the same wires. In some cases ($n = 6$), cells were present on other wires in the bundle. For all these neurons, spike-triggered averaging of LFP suggested that they fired at a preferential phase of beta and/or gamma band oscillations (supplemental Fig. S3, available at www.jneurosci.org as supplemental material). However, although the electrodes were all in a single bundle, the exact spatial relationship between the LFP and neuronal recording locations was not known. Therefore, to further assess the extent to which neurons in GP fire in relation to locally recorded LFP signals, we implanted tetrodes into GP of another group of three rats and analyzed spike and LFP data acquired from wideband recordings obtained from the same tetrodes. Example phase histograms are shown in supplemental Figure S4 (available at www.jneurosci.org as supplemental material). From 19 neurons, 14 (74%) showed significant entrainment to LFP ($p <$ 0.05, Rayleigh's test for homogeneity), with five linked to both gamma and beta, five to gamma only, and four to beta frequency oscillations.

Interplay between frequency bands within GP LFP

Figure 1*C* shows a short section of typical recording from one rat filtered at 0.1–8, 12–30, and 55–65 Hz bands, during which the amplitude of oscillations (the power) in the separate bands can be seen to fluctuate in specific relation to each other. In particular, when β_{14} is high amplitude, γ_{60} tends to be low and vice versa, i.e., power in the two bands appears to be negatively correlated. Quantitative analysis confirmed that this was a significant feature in all rats. For this, we applied a power correlation analysis (Masimore et al., 2004; Fogelson et al., 2005), which returns the correlation coefficient between every possible pair of frequencies. An example analysis for one rat is shown in Figure 1*D*, which reveals a clear, significant negative correlation between narrow frequency bands centered at ≈14 and ≈60 Hz. All rats ($n = 9$) revealed similar significant interactions. No other frequency pairs were significantly positively or negatively correlated in >50% of animals, apart from the expected high positive correlation on and close to the diagonal (i.e., correlation of a frequency with itself and the neighboring frequencies).

Switching between beta and gamma dominance is predicted by delta phase

If a hierarchical organization of LFP frequency bands exists in basal ganglia, then the power fluctuations observed in γ_{60} and β_{14} may be related to oscillations at lower frequencies. To explore

this, we first tested whether fluctuations in γ_{60} and β_{14} power, as expressed in the shape of their AC, can be predicted by Gabor functions derived from different damping frequency terms (see Materials and Methods). Our hypothesis was that, if the predicted AC derived from a damped sinusoid can fit the actual AC, then the damping frequency or frequencies that provided the best fit with the actual data would be candidates for playing a part in such a hierarchy. The 100 × 100 matrices in Figure 2*A* show the Spearman's correlation of the actual AC for γ_{60} and β_{14} bands, with all the Gabor-predicted AC derived for each combination of f_o and f_d terms, averaged across animals ($n = 9$ rats). The data clearly show maximum correlation values for f_o terms close to 14 and 60 Hz, as would be expected. More interestingly, for both γ_{60} and β_{14}, the damping term (f_d) with the highest correlation occurred in the delta range, with maxima centered on f_d values of ≈2–3 Hz. We defined this frequency as δ_3. An illustrative example showing time course of the damping of the AC for γ_{60} and β_{14} compared with the duration of δ_3 AC, the overlap between the actual and predicted AC, and the associated scatter plots for a single animal is shown in Figure 2*B*, using $f_d = 3$ Hz. Both predicted and actual AC for both frequencies can be seen to decrement within the temporal envelope defined by the δ_3 AC function.

The Gabor analysis indicates a potential relationship between δ_3 and each of the two frequencies that were negatively correlated with each other. Another aspect of interest is whether the negative correlation itself could also be related to δ_3. For instance, in the example data trace in Figure 1*C*, periods of high-amplitude β_{14} tended to be at high amplitude within delta band peaks, whereas γ_{60} amplitude appeared to increase during delta troughs. To determine whether such nesting of power fluctuations in each band within different and specific phases of delta rhythm was indeed a significant characteristic of the data, we computed PETPS (Fig. 3). This analysis reveals the timing of fluctuations in β_{14} and γ_{60} with respect to the time of delta troughs (see Materials and Methods).

An example PETPS analysis from one animal is shown in Figure 3*A*. In this example, it can once again be seen that power in β_{14} and γ_{60} fluctuates in anti-phase and that β_{14} is at maximum power during delta peaks, whereas γ_{60} power maxima are synchronous with the triggering δ_3 trough. These timing relationships were consistent across animals, as shown by the normalized group data from the PETPS analysis shown in Figure 3*B* and confirmed by the statistical analysis illustrated in Figure 3*C*. For this, we computed the delta phase at which maximum power was found for β_{14} and γ_{60}. Across all animals, the distribution of maximum power for both these frequencies was significantly clustered at specific phases ($p < 0.05$, Rayleigh's test), and the phase position of the clusters for γ_{60} and β_{14} were significantly different from each other (Watson's U^2 test). As a negative control, we also analyzed a third frequency, 40 Hz, which showed no peak in the power spectral density (Fig. 1*B*) and was not involved in any significant interfrequency interactions (Fig. 1*D*). In contrast to γ_{60} and β_{14}, the trough-triggered average for this frequency was relatively flat (Fig. 3*B*), and the distribution of 40 Hz power maxima was not significantly different from random (Fig. 3*C*).

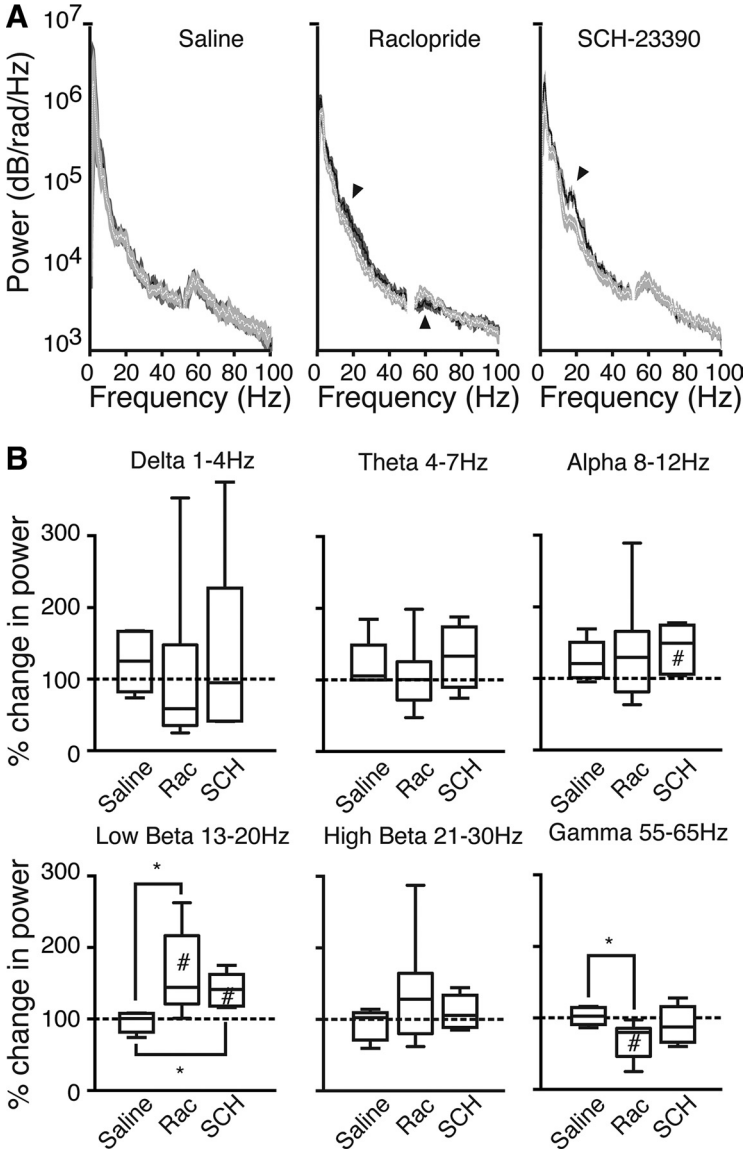

Figure 4. D_1 and D_2 receptor antagonists differentially modulate oscillations in beta and gamma bands. ***A***, Mean ± SEM power spectral density, from before injection (white line and light gray shading) and after injection (black line, dark gray shading) of saline, raclopride, or SCH23390. Arrowheads indicate significant deviations of post-injection from pre-injection data, quantified in ***B***. ***B***, Box plots show predrug–postdrug power ratios in different frequency bands for saline ($n = 6$), raclopride (Rac; $n = 9$), and SCH23390 (SCH; $n = 6$) treatments. $^{\#}p < 0.05$ compared with 1:1; $^{*}p < 0.05$ compared with saline treatment.

Oscillation power and interfrequency interplay is under control of dopamine through differential actions at D_1 and D_2 receptors

We investigated the role of endogenous dopamine in regulating the interfrequency dependencies described in the previous sections, by administering the selective dopamine D_1 and D_2 receptor

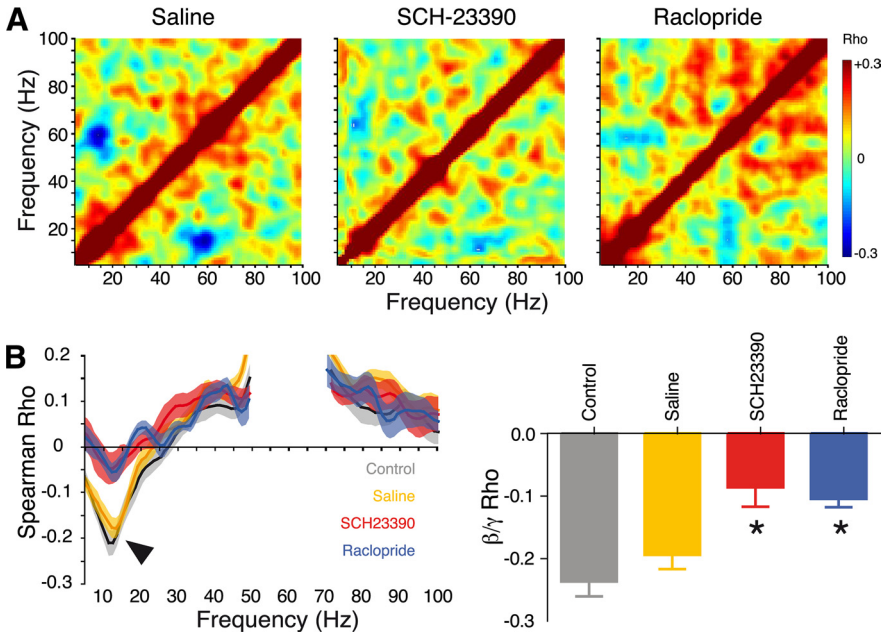

Figure 5. Dopamine antagonists downregulate the negative correlation between beta and gamma power. ***A***, Example data. Matrices show Spearman's ρ correlation coefficient (color scale) for all frequency pairs, for one rat, after saline, SCH23390, or raclopride injection. ***B***, Group data. Color bands show the average ± SEM Spearman's ρ correlation between γ_{60} and other frequencies (5–100 Hz), before injection of saline (control, gray) and after injection of saline (yellow), SCH23390 (red), or raclopride (blue). Arrowhead indicates negative correlation with the beta band before and after saline injection. Histogram shows mean ± SEM Spearman's ρ for the maximum negative correlation between γ_{60} and frequencies in the 10–30 Hz band, in each condition. *$p < 0.001$ compared with saline.

antagonists SCH23390 and raclopride. Six animals were tested with raclopride, SCH23390, and vehicle and an additional three with raclopride only. Doses were selected such that the drugs generated similar levels of mild catalepsy, confirmed by elevated bar test times (mean ± SEM bar time: raclopride, 18 ± 6 s; SCH23390, 25 ± 9 s) compared with saline control injections, in which bar times were <1 s and so scored as 0 s in all cases ($p < 0.05$, paired t test, $n = 6$).

We first determined the effect of dopamine antagonists on LFP PSD. Example traces are shown in supplemental Figure S1 (available at www.jneurosci.org as supplemental material). Analysis of group data, shown in Figure 4*A*, revealed that drug treatments altered the amplitude of PSD peaks, without altering their characteristic frequency. The specific effects depended on the drug and the frequency band. Both drugs elevated the spectral density over the beta range. In contrast, only raclopride influenced the low gamma peak, and the effect was to flatten it compared with the predrug control. These observations were confirmed in the quantitative analysis shown in Figure 4*B*. For this, beta was divided into low and high beta sub-bands, and quantification of gamma was restricted to the low gamma subband that exhibited the peak in the control PSD. Other classically defined delta, theta, and alpha bands were included for comparison. There was a significant effect of treatment (Kruskal–Wallis test, $p < 0.05$), and *post hoc* tests confirmed that this was attributable to significant elevation in low beta power by both drugs compared with saline and significant depression of low gamma power by the D_2 receptor antagonist raclopride but not SCH23390 ($p < 0.05$, Wilcoxon's signed rank test).

The box plots in Figure 4*B* also suggested the possibility of a trend toward increases in alpha power after all treatments, including saline. However, one-sample (Wilcoxon's signed rank) tests showed that the only point that was significantly different from no change was alpha band power after SCH23390 injection ($p < 0.05$), and this value was not significantly different from the post-injection values for saline or raclopride. These results suggest the possibility of a small nonspecific effect on alpha power from some aspect of the drug administration procedure itself.

Finally, we asked whether constitutive dopamine has a role in modulating interplay between gamma and beta and nesting within delta frequency bands. First, we compared power correlation matrices across drug treatments. Figure 5*A* shows example post-injection data from one animal. The post-saline matrix shows the same pattern as seen in Figure 1*D* for the predrug condition, with clear negative correlation in power between γ_{60} and β_{14}. In contrast, the negative correlation almost completely disappeared after administration of either dopamine antagonist. This was confirmed in the quantitative analysis of group data shown in Figure 5*B*. Both raclopride and SCH23390 significantly reduced the mean value of the Spearman's correlation coefficient between power at γ_{60} and β_{14} ($p < 0.05$).

Second, to determine whether SCH23390 and raclopride differentially affected the nesting of β_{14} and γ_{60} within δ_3, we analyzed PETPS under the different pharmacological conditions, as shown in Figure 6. This analysis revealed that the D_1 and D_2 antagonists affected power modulation and correlation patterns in a complex manner, which was differential both across frequencies, and between drugs. For the γ_{60} band, inspection of the plots in Figure 6*A* reveals that administration of the D_2 antagonist SCH23390 completely reversed the phase relationship, confirmed by a significant shift in the position of the delta phase of the maximum power (Fig. 6*B*). As illustrated in Figure 6*B*, before injection the phase of γ_{60} maximum power was significantly clustered at ≈0° (i.e., at the time of the δ_3 trough), but after SCH23390, it was significantly clustered at ≈180°, i.e., the time of the δ_3 peaks surrounding the troughs ($p < 0.05$, Rayleigh's test). This new cluster position was furthermore significantly different from predrug ($p < 0.05$, Watson's U^2 test). In contrast, the D_2 antagonist raclopride had no effect on the relationship of γ_{60} power with δ_3. The data in Figure 6 also reveal that drug effects were quite different for the β_{14} band. Here, both drugs simply eliminated the relationship of β_{14} power fluctuations with γ_{60} phase, so that normalized data plots (Fig. 6*A*) became flat and the position of power maxima became randomly scattered with respect to δ_3 phase (Fig. 6*B*). It is important to recall that this loss of temporal relationship was in the face of a significant increase in mean β_{14} power. Saline administration did not affect the temporal patterning of power for either band.

Discussion

The main findings of the present study are summarized in Figure 7. First, we found that power in beta and gamma LFP bands is negatively correlated in rat GP, in resting animals. Second, we show that the modulation of beta and gamma power is nested within slow oscillations in the delta frequency band, with peak

power in β_{14} and γ_{60} at different phases of δ_3. Third, endogenous dopamine is a critical determinant of not only the total power in each of the bands but also the negative correlation between beta and gamma power, and the relationship power in these bands to delta phase, with differential roles for D_2 and D_1 receptors.

Although volume conduction of signals from distant sources cannot be ruled out, particularly for structures such as basal ganglia nuclei that lack a layered structure (Berke, 2009), we found that the majority of neurons recorded on the GP electrodes showed phase locking of activity to LFP oscillations. This entrainment of spiking to the LFP indicates that the rhythms recorded in the LFP waves at least partially reflect local electrophysiological phenomena. Some previous data showing enhanced coherence at gamma frequencies between GP and other structures in anesthetized rats (but during periods of cortical activation considered physiologically similar to the awake state) also support a local component to LFP signals recorded in GP (Magill et al., 2004; Sharott et al., 2005). There is also considerable evidence for expression of anesthetic-induced slow-wave activity in rat GP (Magill et al., 2004; Walters et al., 2007; Zold et al., 2007). How the local rhythms are generated remains uncertain, but cocultures of GP and STN neurons form networks that show intrinsic slow oscillations (Plenz and Kital, 1999), suggesting that basal ganglia networks including GP have the necessary machinery to generate such rhythms, and modeling studies indicate that the properties of the intact GP–STN network would support oscillations in both the beta (Holgado et al., 2010) and gamma (Humphries et al., 2006) ranges.

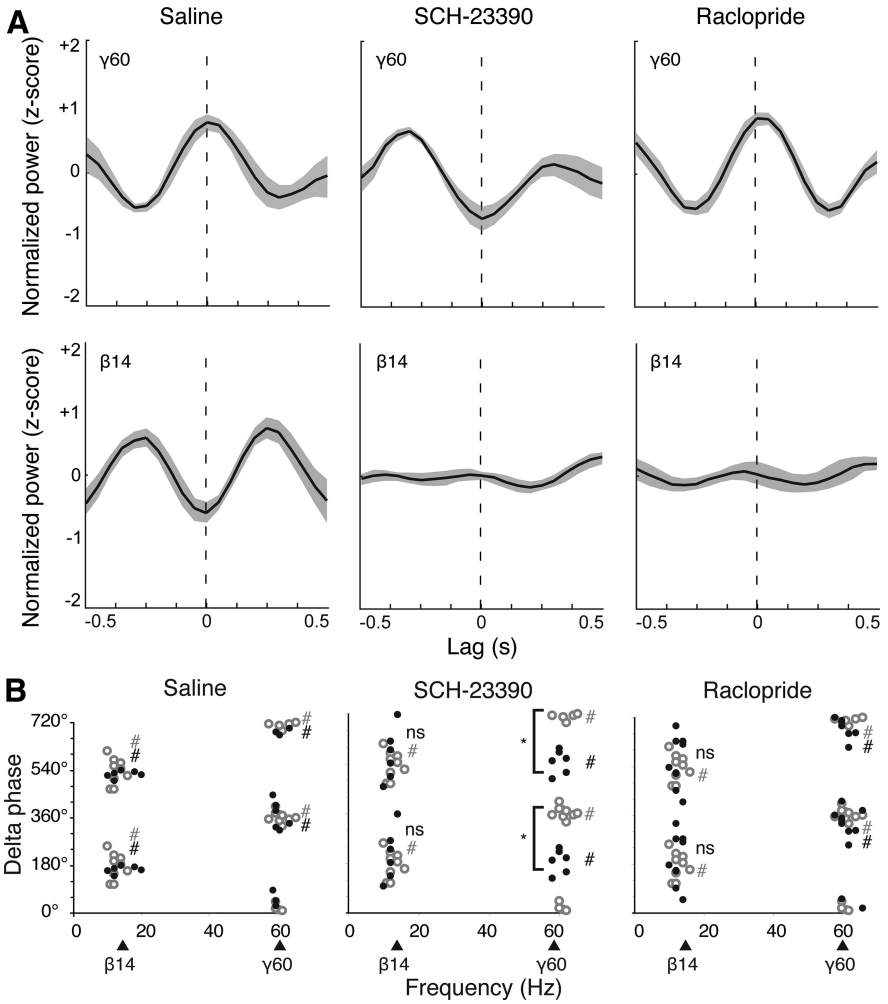

Figure 6. Dopamine antagonists alter nesting of beta and gamma power fluctuations within delta. ***A***, Mean ± SEM normalized PETPS, triggered on δ_3 trough after saline or drug (SCH23390 or raclopride) injection, for γ_{60} (above) and β_{14} bands (below). ***B***, Points show the δ_3 phase at which maximum power occurs in β_{14} and γ_{60} bands, for each animal before (gray circles) and after saline or drug injection (black circles). $^{\#}p < 0.05$ compared with random distribution; $^{*}p < 0.05$ comparing phase distributions before and after injection. ns, Not significant.

Nesting of negative beta–gamma power correlation within delta rhythm

A main finding of the present study is that moment-to-moment alternation (negative correlation) of power in beta and gamma bands is a feature of activity in basal ganglia of intact rat. This is consistent with findings in L-3,4-dihydroxyphenylalanine-treated Parkinson's patients (Fogelson et al., 2005) and suggests that there may be a fundamental linkage of the neural generators underlying beta and gamma frequency oscillations.

Furthermore, we found the periods of negatively correlated power fluctuations in beta and gamma bands to exist over short time frames that were defined by (nested within) delta phase. These data from unanesthetized rats therefore support and extend previous evidence for nesting of basal ganglia gamma within slower oscillations, in striatum and pedunculopontine tegmental nucleus of anesthetized rats (Stern et al., 1997; Mena-Segovia et al., 2008) and striatum of unanesthetized rats after amphetamine administration (Berke, 2009) or during navigation tasks (Tort et al., 2008). Nesting of gamma within lower-frequency waves is well known in cortico-hippocampal networks and is thought to arise from the interaction of inputs oscillating at low frequency with local circuit mechanisms for generation of higher-frequency oscillations (Bragin et al., 1995). It is plausible to imagine that similar processes operate through the basal ganglia network.

It is well known that beta and gamma in the cortex–basal ganglia network are modulated according to movement state (Bergman et al., 1994; Donoghue et al., 1998; Brown and Marsden, 1999; Aoki et al., 2001; Brown et al., 2001, 2002; Cassidy et al., 2002; Levy et al., 2002; Lee, 2003; Masimore et al., 2005; Sharott et al., 2005; van der Meer and Redish, 2009). In contrast, the present results, and data showing negative power correlation between beta and gamma bands in humans (Fogelson et al., 2005), were obtained at rest. Thus, beta–gamma alternation may be a default baseline state in the basal ganglia. However, movement may bring out additional complexity; for instance, it has been shown recently that specific movement tasks enhance activity in a higher-frequency band within gamma (Berke, 2009).

Whereas we found the nesting frequency to center in the delta band, studies of nesting of gamma in hippocampus and cortical networks emphasize the role played by slightly higher (theta) frequencies (Bragin et al., 1995; Chrobak and Buzsáki, 1998;

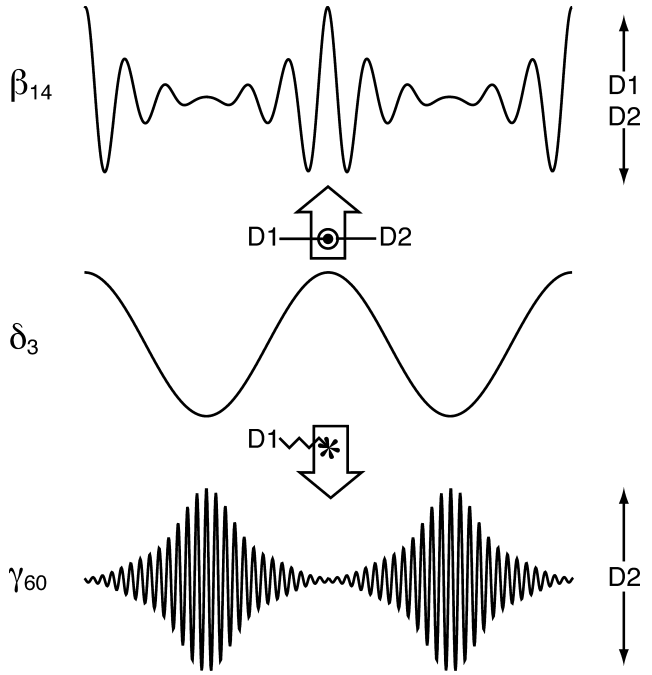

Figure 7. Diagram summarizing hierarchical organization of dopamine-dependent frequency interplay within rat GP. Line arrows (right side) indicate dependence of β_{14} mean power on both D_1 and D_2 dopamine receptors and of γ_{60} mean power on D_2 receptors alone. Block arrows highlight the temporal relationship between δ_3 phase and fluctuations of power in γ_{60} and β_{14}, which are in anti-phase relative to each other. The differential modulation of the temporal relationships with δ_3 by dopamine receptor subtypes is also indicated; lines terminating in circles indicate effect on strength, whereas zigzag line terminating in asterisk indicates an effect on phase of the relationship.

Lakatos et al., 2005; Canolty et al., 2006; Sirota et al., 2008). However, similar to the present finding, activity at lower frequencies in the delta range has also been shown to form the base of a complex "oscillatory hierarchy" in auditory cortex of conscious monkeys, in which delta oscillations modulate theta, which in turn modulates gamma band activity (Lakatos et al., 2005).

It has been suggested that the function of interfrequency nesting recorded elsewhere in the brain may be to allow spatially distributed subpopulations to form temporally defined ensembles through the action of propagating slow oscillations (Chrobak and Buzsáki, 1998) or to modulate excitability to optimize processing of rhythmic inputs (Lakatos et al., 2005). In basal ganglia, an additional possible functional role for nesting might be to organize interfrequency phase–amplitude relationships. We found that beta and gamma fluctuated in amplitude in antiphase relative to specific phases of delta waves so that beta and gamma amplitude were locked in a delicate temporal counterpoint. Such conjoint nesting of dual frequencies does not appear to have been reported previously and presumably reflects the special importance of beta–gamma interactions in basal ganglia functions (Brown, 2003; Gatev et al., 2006; van der Meer and Redish, 2009). Propagating delta waves therefore appear to lie at the base of an oscillatory hierarchy that may be critical for organizing functional states within the basal ganglia–cortex loop.

Dopamine dependence of frequency power interactions: different roles of D_1 and D_2 receptors

Activity through basal ganglia pathways is strongly modulated by dopamine acting within the striatum and also to some extent directly in STN and GP (Smith et al., 1998; Gauthier et al., 1999). During hypokinesia induced by blockade of endogenous dopamine action at either D_1 or D_2 receptors with SCH23390 or raclopride, respectively, we found changes in multiple LFP measures, including power in different frequency bands, the correlation in power between bands, and the nesting of this correlation according to delta phase. Changes in neural circuit activity could in principle be secondary to, rather than causative of, changes in motility. However, this is unlikely to account for the findings here, because the two drugs had differential effects on power and interfrequency correlations, despite having similar effects on movement.

Given the difference in relative abundance of the two receptor subtypes in the direct (dominated by D_1) and indirect (dominated by D_2) pathways, differential effects of blockade of these receptors might indicate differing functional roles of the two pathways in the modulations seen in LFP recorded from GP. Effects on beta frequency were relatively straightforward. Both D_1 and D_2 antagonists acutely increased low-beta power in the GP. This is consistent with some previous acute studies (Sebban et al., 1999; Dejean et al., 2009) and with the idea that beta power is linked to akinetic states, although increases in beta power appear to be much more robust in chronic lesion rat models of Parkinson's disease (Sharott et al., 2005).

Furthermore, both antagonists abolished the entrainment of beta power fluctuation to the phase of δ_3. Given the fact that the negative correlation observed between beta and gamma power appears to reflect an inverse relationship of the two frequency bands to delta, it is not surprising that the abolition of nesting of beta was accompanied by elimination of the negative correlation between beta and gamma frequencies that is observed in control conditions.

Although the underlying mechanisms relating beta power to delta phase remain uncertain, these data raise the possibility that the loss of entrainment to delta phase could be causally linked to the increase in beta power that was seen. Decoupling beta power from a temporal constraint provided by delta rhythms could enable beta power to remain at abnormally high levels for protracted periods and thus contribute to the exaggeration of beta oscillations seen in virtually all structures of the basal ganglia–cortex loop in parkinsonism (Hammond et al., 2007). Whatever the case, because beta power and beta–delta nesting in GP are equally affected by both dopamine receptor subtypes, these parameters are unlikely to be specifically modulated by indirect pathway activity limited to GP but may be more generally related to changes in capacity for movement, generated elsewhere in the basal ganglia–cortex circuit after disruption of dopamine transmission.

In contrast to the nonspecific effects of dopamine antagonists on beta power, we found that power in the gamma band was only affected significantly after administration of the D_2 antagonist raclopride, with no change after SCH23390, despite both drugs resulting in similar levels of akinesia. Gamma recorded from the STN, which is strongly interconnected with GP in the indirect pathway (Smith et al., 1998; Bevan et al., 2007), is also modulated by D_2 receptor (Brown et al., 2002). Together, these data support the idea that gamma in GP reflects a specific function of local circuit interactions within the indirect pathway (Bevan et al., 2002), as suggested by basal ganglia simulations (Humphries et al., 2006). Constitutive dopamine acting on the D_2 receptor tends to decrease neural excitability (Surmeier et al., 2007), so raclopride is expected to increase the excitability of indirect pathway neurons projecting to GP. The resulting increased inhibitory input to GP could be responsible for lowering gamma power, for instance, by modulating local circuit interactions between GP

and STN involved in generating local gamma (Humphries et al., 2006).

Although raclopride reduced average gamma power, our analysis revealed that mechanisms linking gamma power fluctuations with delta phase remained intact, because the remaining gamma activity was still nested within delta. These data suggest that the nesting mechanism does not depend on dopamine acting via D_2-receptor-bearing elements of the indirect pathway. Instead, D_1 antagonism had a dramatic effect, reversing the phase of delta at which gamma was at maximum, indicating that D_1-receptor-expressing direct pathway neurons may be more involved in regulating the nesting phenomenon. Direct pathway neurons could modulate the gamma in GP indirectly, by altering thalamocortical loop activity that in turn feeds back into striatal and STN networks. More directly, some D_1-expressing striatal neurons have axon collaterals that innervate the GP, which could play a more local role in this switching (Kawaguchi et al., 1990; Wu et al., 2000; Deng et al., 2006).

References

Aoki F, Fetz EE, Shupe L, Lettich E, Ojemann GA (2001) Changes in power and coherence of brain activity in human sensorimotor cortex during performance of visuomotor tasks. Biosystems 63:89–99.

Bergman H, Wichmann T, Karmon B, DeLong MR (1994) The primate subthalamic nucleus. II. Neuronal activity in the MPTP model of parkinsonism. J Neurophysiol 72:507–520.

Berke JD (2009) Fast oscillations in cortical-striatal networks switch frequency following rewarding events and stimulant drugs. Eur J Neurosci 30:848–859.

Berke JD, Okatan M, Skurski J, Eichenbaum HB (2004) Oscillatory entrainment of striatal neurons in freely moving rats. Neuron 43:883–896.

Bevan MD, Magill PJ, Terman D, Bolam JP, Wilson CJ (2002) Move to the rhythm: oscillations in the subthalamic nucleus-external globus pallidus network. Trends Neurosci 25:525–531.

Bevan MD, Hallworth NE, Baufreton J (2007) GABAergic control of the subthalamic nucleus. Prog Brain Res 160:173–188.

Bischoff S, Heinrich M, Sonntag JM, Krauss J (1986) The D-1 dopamine receptor antagonist SCH 23390 also interacts potently with brain serotonin (5-HT2) receptors. Eur J Pharmacol 129:367–370.

Bragin A, Jandó G, Nádasdy Z, Hetke J, Wise K, Buzsáki G (1995) Gamma (40–100 Hz) oscillation in the hippocampus of the behaving rat. J Neurosci 15:47–60.

Brown P (2003) Oscillatory nature of human basal ganglia activity: relationship to the pathophysiology of Parkinson's disease. Mov Disord 18:357–363.

Brown P, Marsden CD (1999) Bradykinesia and impairment of EEG desynchronization in Parkinson's disease. Mov Disord 14:423–429.

Brown P, Oliviero A, Mazzone P, Insola A, Tonali P, Di Lazzaro V (2001) Dopamine dependency of oscillations between subthalamic nucleus and pallidum in Parkinson's disease. J Neurosci 21:1033–1038.

Brown P, Kupsch A, Magill PJ, Sharott A, Harnack D, Meissner W (2002) Oscillatory local field potentials recorded from the subthalamic nucleus of the alert rat. Exp Neurol 177:581–585.

Buzsáki G, Bragin A, Chrobak JJ, Nadasdy Z, Sik A, Hsu M, Ylinen A (1994) Oscillatory and intermittent synchrony in the hippocampus: Relevance to memory trace formation. In: Temporal coding in the brain (Buzsáki G, Llinas R, Singer W, Berthoz A, Christen Y, eds), pp 145–172. Berlin: Springer.

Canolty RT, Edwards E, Dalal SS, Soltani M, Nagarajan SS, Kirsch HE, Berger MS, Barbaro NM, Knight RT (2006) High gamma power is phase-locked to theta oscillations in human neocortex. Science 313:1626–1628.

Cassidy M, Mazzone P, Oliviero A, Insola A, Tonali P, Di Lazzaro V, Brown P (2002) Movement-related changes in synchronization in the human basal ganglia. Brain 125:1235–1246.

Chrobak JJ, Buzsáki G (1998) Gamma oscillations in the entorhinal cortex of the freely behaving rat. J Neurosci 18:388–398.

Courtemanche R, Fujii N, Graybiel AM (2003) Synchronous, focally modulated beta-band oscillations characterize local field potential activity in the striatum of awake behaving monkeys. J Neurosci 23:11741–11752.

Dejean C, Hyland B, Arbuthnott G (2009) Cortical effects of subthalamic stimulation correlate with behavioral recovery from dopamine antagonist induced akinesia. Cereb Cortex 19:1055–1063.

Deng YP, Lei WL, Reiner A (2006) Differential perikaryal localization in rats of D1 and D2 dopamine receptors on striatal projection neuron types identified by retrograde labeling. J Chem Neuroanat 32:101–116.

Donoghue JP, Sanes JN, Hatsopoulos NG, Gaál G (1998) Neural discharge and local field potential oscillations in primate motor cortex during voluntary movements. J Neurophysiol 79:159–173.

Engel AK, König P, Gray CM, Singer W (1990) Stimulus-dependent neuronal oscillations in cat visual cortex: inter-columnar interaction as determined by cross-correlation analysis. Eur J Neurosci 2:588–606.

Fisher NI (1993) Statistical analysis of circular data. Cambridge, UK: Cambridge UP.

Fogelson N, Pogosyan A, Kühn AA, Kupsch A, van Bruggen G, Speelman H, Tijssen M, Quartarone A, Insola A, Mazzone P, Di Lazzaro V, Limousin P, Brown P (2005) Reciprocal interactions between oscillatory activities of different frequencies in the subthalamic region of patients with Parkinson's disease. Eur J Neurosci 22:257–266.

Fries P, Schröder JH, Roelfsema PR, Singer W, Engel AK (2002) Oscillatory neuronal synchronization in primary visual cortex as a correlate of stimulus selection. J Neurosci 22:3739–3754.

Fries P, Nikolić D, Singer W (2007) The gamma cycle. Trends Neurosci 30:309–316.

Gatev P, Darbin O, Wichmann T (2006) Oscillations in the basal ganglia under normal conditions and in movement disorders. Mov Disord 21:1566–1577.

Gauthier J, Parent M, Lévesque M, Parent A (1999) The axonal arborization of single nigrostriatal neurons in rats. Brain Res 834:228–232.

Gray CM, König P, Engel AK, Singer W (1989) Oscillatory responses in cat visual cortex exhibit inter-columnar synchronization which reflects global stimulus properties. Nature 338:334–337.

Hammond C, Bergman H, Brown P (2007) Pathological synchronization in Parkinson's disease: networks, models and treatments. Trends Neurosci 30:357–364.

Holgado AJ, Terry JR, Bogacz R (2010) Conditions for the generation of beta oscillations in the subthalamic nucleus–globus pallidus network. J Neurosci 30:12340–12352.

Humphries MD, Stewart RD, Gurney KN (2006) A physiologically plausible model of action selection and oscillatory activity in the basal ganglia. J Neurosci 26:12921–12942.

Isomura Y, Sirota A, Ozen S, Montgomery S, Mizuseki K, Henze DA, Buzsáki G (2006) Integration and segregation of activity in entorhinal-hippocampal subregions by neocortical slow oscillations. Neuron 52:871–882.

Kawaguchi Y, Wilson CJ, Emson PC (1990) Projection subtypes of rat neostriatal matrix cells revealed by intracellular injection of biocytin. J Neurosci 10:3421–3438.

Lakatos P, Shah AS, Knuth KH, Ulbert I, Karmos G, Schroeder CE (2005) An oscillatory hierarchy controlling neuronal excitability and stimulus processing in the auditory cortex. J Neurophysiol 94:1904–1911.

Lee D (2003) Coherent oscillations in neuronal activity of the supplementary motor area during a visuomotor task. J Neurosci 23:6798–6809.

Levy R, Ashby P, Hutchison WD, Lang AE, Lozano AM, Dostrovsky JO (2002) Dependence of subthalamic nucleus oscillations on movement and dopamine in Parkinson's disease. Brain 125:1196–1209.

Magill PJ, Sharott A, Bolam JP, Brown P (2004) Brain state-dependency of coherent oscillatory activity in the cerebral cortex and basal ganglia of the rat. J Neurophysiol 92:2122–2136.

Marin C, Parashos SA, Kapitzoglou-Logothetis V, Peppe A, Chase TN (1993) D1 and D2 dopamine receptor-mediated mechanisms and behavioral supersensitivity. Pharmacol Biochem Behav 45:195–200.

Masimore B, Kakalios J, Redish AD (2004) Measuring fundamental frequencies in local field potentials. J Neurosci Methods 138:97–105.

Masimore B, Schmitzer-Torbert NC, Kakalios J, Redish AD (2005) Transient striatal gamma local field potentials signal movement initiation in rats. Neuroreport 16:2021–2024.

Mena-Segovia J, Sims HM, Magill PJ, Bolam JP (2008) Cholinergic brainstem neurons modulate cortical gamma activity during slow oscillations. J Physiol 586:2947–2960.

Nargeot R, Petrissans C, Simmers J (2007) Behavioral and *in vitro* correlates of compulsive-like food seeking induced by operant conditioning in *Aplysia*. J Neurosci 27:8059–8070.

Paxinos G, Watson C (1997) The rat brain in stereotaxic coordinates, Ed 3. London: Academic.

Plenz D, Kital ST (1999) A basal ganglia pacemaker formed by the subthalamic nucleus and external globus pallidus. Nature 400:677–682.

Sebban C, Zhang XQ, Tesolin-Decros B, Millan MJ, Spedding M (1999) Changes in EEG spectral power in the prefrontal cortex of conscious rats elicited by drugs interacting with dopaminergic and noradrenergic transmission. Br J Pharmacol 128:1045–1054.

Sharott A, Magill PJ, Harnack D, Kupsch A, Meissner W, Brown P (2005) Dopamine depletion increases the power and coherence of beta-oscillations in the cerebral cortex and subthalamic nucleus of the awake rat. Eur J Neurosci 21:1413–1422.

Singer W (2001) Consciousness and the binding problem. Ann N Y Acad Sci 929:123–146.

Sirota A, Buzsáki G (2005) Interaction between neocortical and hippocampal networks via slow oscillations. Thalamus Relat Syst 3:245–259.

Sirota A, Montgomery S, Fujisawa S, Isomura Y, Zugaro M, Buzsáki G (2008) Entrainment of neocortical neurons and gamma oscillations by the hippocampal theta rhythm. Neuron 60:683–697.

Smith Y, Bevan MD, Shink E, Bolam JP (1998) Microcircuitry of the direct and indirect pathways of the basal ganglia. Neuroscience 86:353–387.

Stern EA, Kincaid AE, Wilson CJ (1997) Spontaneous subthreshold membrane potential fluctuations and action potential variability of rat corticostriatal and striatal neurons in vivo. J Neurophysiol 77:1697–1715.

Surmeier DJ, Ding J, Day M, Wang Z, Shen W (2007) D1 and D2 dopamine-receptor modulation of striatal glutamatergic signaling in striatal medium spiny neurons. Trends Neurosci 30:228–235.

Tort AB, Kramer MA, Thorn C, Gibson DJ, Kubota Y, Graybiel AM, Kopell NJ (2008) Dynamic cross-frequency couplings of local field potential oscillations in rat striatum and hippocampus during performance of a T-maze task. Proc Natl Acad Sci U S A 105:20517–20522.

van der Meer MA, Redish AD (2009) Low and high gamma oscillations in rat ventral striatum have distinct relationships to behavior, reward, and spiking activity on a learned spatial decision task. Front Integr Neurosci 3:9.

Walters JR, Hu D, Itoga CA, Parr-Brownlie LC, Bergstrom DA (2007) Phase relationships support a role for coordinated activity in the indirect pathway in organizing slow oscillations in basal ganglia output after loss of dopamine. Neuroscience 144:762–776.

Wu Y, Richard S, Parent A (2000) The organization of the striatal output system: a single-cell juxtacellular labeling study in the rat. Neurosci Res 38:49–62.

Young MP, Tanaka K, Yamane S (1992) On oscillating neuronal responses in the visual cortex of the monkey. J Neurophysiol 67:1464–1474.

Zold CL, Ballion B, Riquelme LA, Gonon F, Murer MG (2007) Nigrostriatal lesion induces D2-modulated phase-locked activity in the basal ganglia of rats. Eur J Neurosci 25:2131–2144.